

# 1 Evaluation of CMIP6 model simulations of PM<sub>2.5</sub> and its 2 components over China

3 Fangxuan Ren<sup>1</sup>, Jintai Lin<sup>1</sup>, Chenghao Xu<sup>1</sup>, Jamiu A. Adeniran<sup>1</sup>, Jingxu Wang<sup>2</sup>,  
4 Randall V. Martin<sup>3</sup>, Aaron van Donkelaar<sup>3</sup>, Melanie S. Hammer<sup>4</sup>, Larry W. Horowitz<sup>5</sup>,  
5 Steven T. Turnock<sup>6,7</sup>, Naga Oshima<sup>8</sup>, Jie Zhang<sup>9</sup>, Susanne Bauer<sup>10</sup>, Kostas  
6 Tsigaridis<sup>11,10</sup>, Øyvind Seland<sup>12</sup>, Pierre Nabat<sup>13</sup>, David Neubauer<sup>14</sup>, Gary Strand<sup>15</sup>,  
7 Twan van Noije<sup>16</sup>, Philippe Le Sager<sup>16</sup>, Toshihiko Takemura<sup>17</sup>

8 <sup>1</sup> Laboratory for Climate and Ocean-Atmosphere Studies, Department of Atmospheric and Oceanic  
9 Sciences, School of Physics, Peking University, Beijing 100871, China

10 <sup>2</sup> Frontier Science Center for Deep Ocean Multispheres and Earth System (FDOMES) and Physical  
11 Oceanography Laboratory, College of Oceanic and Atmospheric Sciences, Ocean University of China,  
12 Qingdao 266100, China

13 <sup>3</sup> Department of Energy, Environmental, and Chemical Engineering, Washington University, St. Louis,  
14 MO, USA

15 <sup>4</sup> St. Francis Xavier University, Department of Earth Sciences, Antigonish, NS, Canada

16 <sup>5</sup> NOAA Geophysical Fluid Dynamics Laboratory, Princeton, NJ, USA

17 <sup>6</sup> Met Office Hadley Center, Exeter, UK

18 <sup>7</sup> University of Leeds Met Office Strategic (LUMOS) Research Group, University of Leeds, UK

19 <sup>8</sup> Meteorological Research Institute, Tsukuba, Japan

20 <sup>9</sup> Beijing Climate Center, China Meteorological Administration, Beijing 100081, China

21 <sup>10</sup> NASA Goddard Institute for Space Studies, New York, NY, USA

22 <sup>11</sup> Center for Climate Systems Research, Columbia University, New York, NY, USA

23 <sup>12</sup> Norwegian Meteorological Institute, P.O. Box 43 Blindern, Oslo, Norway

24 <sup>13</sup> Centre National de Recherches Météorologiques (CNRM), Météo-France, CNRS, Toulouse, France

25 <sup>14</sup> Institute of Atmospheric and Climate Science, ETH Zurich, Zurich, Switzerland

26 <sup>15</sup> Climate and Global Dynamics Laboratory, the National Center for Atmospheric Research, Boulder,  
27 CO, USA

28 <sup>16</sup> Royal Netherlands Meteorological Institute, De Bilt, Netherlands

29 <sup>17</sup> Research Institute for Applied Mechanics, Kyushu University, Fukuoka, Japan

30 *Correspondence to:* Jintai Lin (linjt@pku.edu.cn)

31 **Abstract.** Earth system models (ESMs) participating in the latest Coupled Model Intercomparison  
32 Project Phase 6 (CMIP6) simulate various components of fine particulate matter (PM<sub>2.5</sub>) as major climate  
33 forcers. Yet the model performance for PM<sub>2.5</sub> components remains little evaluated due in part to lack of  
34 observational data. Here, we evaluate near-surface concentrations of PM<sub>2.5</sub> and its five main components  
35 over China as simulated by fourteen CMIP6 models, including organic carbon (OC, available in 14  
36 models), black carbon (BC, 14 models), sulfate (14 models), nitrate (4 models), and ammonium (5  
37 models). For this purpose, we collect observational data between 2000 and 2014 from a satellite-based

38 dataset for total  $PM_{2.5}$  and from 2469 measurement records in the literature for  $PM_{2.5}$  components. Seven  
39 models output total  $PM_{2.5}$  concentrations, and they all underestimate the observed total  $PM_{2.5}$  over eastern  
40 China, with GFDL-ESM4 (−1.5%) and MPI-ESM-1-2-HAM (−1.1%) exhibiting the smallest biases  
41 averaged over the whole country. The other seven models, for which we recalculate total  $PM_{2.5}$  from the  
42 available components output, underestimate the total  $PM_{2.5}$  concentrations, partly because of the missing  
43 model representations of nitrate and ammonium. Concentrations of the five individual components are  
44 underestimated in almost all models, except that sulfate is overestimated in MPI-ESM-1-2-HAM by 12.6%  
45 and in MRI-ESM2-0 by 24.5%. The underestimation is the largest for OC (by −71.2% to −37.8% across  
46 the 14 models) and the smallest for BC (−47.9% to −12.1%). The multi-model mean (MMM) reproduces  
47 fairly well the observed spatial pattern for OC ( $R = 0.51$ ), sulfate ( $R = 0.57$ ), nitrate ( $R = 0.70$ ) and  
48 ammonium ( $R = 0.74$ ), yet the agreement is poorer for BC ( $R = 0.39$ ). The varying performances of  
49 ESMs on total  $PM_{2.5}$  and its components have important implications for the modeled magnitude and  
50 spatial pattern of aerosol radiative forcing.

## 51 **1 Introduction**

52 Fine particulate matter ( $PM_{2.5}$ ) influences air quality, human health and climate change. Exposure to near-  
53 surface  $PM_{2.5}$  is associated with millions of global premature deaths each year (Zhang et al., 2017; World  
54 Health Organization, 2021).  $PM_{2.5}$  affects the radiative budget of the climate system directly through  
55 scattering and absorption and indirectly via clouds. The effects of atmospheric aerosols on cloud droplet  
56 concentrations, cloud distributions and radiative properties pose large uncertainties in the estimating  
57 radiative forcing (Carslaw et al., 2013; Seinfeld et al., 2016). Earth system models (ESMs) are essential  
58 tools for studying global climate change. The accuracy of  $PM_{2.5}$  simulations in ESMs exhibits a crucial  
59 constraint on the reliability of these models in climate change simulation and projection. The Coupled  
60 Model Intercomparison Project Phase 6 (CMIP6) provides an opportunity to evaluate simulated  $PM_{2.5}$   
61 and its components by the current-generation ESMs, which implement interactive aerosol and  
62 atmospheric chemistry (Turnock et al., 2020). A total of 21 ESMs participating in CMIP6 provide total  
63  $PM_{2.5}$  and/or several component simulations, although the aerosol component species vary across these  
64 models. Fourteen models include organic aerosol (OA, converted to organic carbon (OC) in this study  
65 by assuming  $OA / OC = 1.6$ ), black carbon (BC), sulfate, dust (DST), and sea salt (SSLT). Four of these

66 14 models also include nitrate and five include ammonium (Table S1).  
67 Aerosol optical depth (AOD) during 2000–2014 simulated in CMIP5 and CMIP6 are in broad agreement  
68 with satellite retrievals over most parts of Europe, North America, and India (Zhang et al., 2022a; Cherian  
69 and Quaas, 2020). CMIP6 models better capture satellite-based AOD trends in western North America  
70 and eastern China, whereas CMIP5 models failed to reproduce the trends in AOD (Mortier et al., 2020;  
71 Cherian and Quaas, 2020). Studies have emerged over recent years to assess the CMIP model  
72 performance of individual aerosol components. An assessment of CMIP5 dust aerosol simulations using  
73 independent data from 1851 to 2011 over North Africa shows a common underestimate (Evan et al.,  
74 2016). Another analysis of CMIP3 and CMIP5 models suggests sea salt aerosols over the tropical Pacific  
75 to be significantly underestimated (Chen et al., 2020). Evaluation of the vertical distribution of BC in  
76 CMIP5 models based on aircraft measurements shows an overestimate in the upper troposphere  
77 especially over the Central Pacific (Allen and Landuyt, 2014). Several CMIP5 models produce high  
78 sulfate burdens over eastern China, the Indian Peninsula and the northern Indo-Chinese Peninsula,  
79 although the transport difference among these models results in distinctive spatial distributions (Li et al.,  
80 2020). Overall, global climate models struggle to accurately reproduce observed aerosol component  
81 concentrations over different world regions.

82 China is a major region with heavy aerosol pollution, dense population and complex climate, and thus it  
83 is critical to understand the performance of ESMs for aerosol simulations over this country. Several  
84 studies have evaluated total PM<sub>2.5</sub> simulations of CMIP models over China, using AOD data from  
85 satellite retrievals (Sokol and Small Griswold, 2017; Michou et al., 2020) and ground-based aerosol  
86 networks (Mortier et al., 2020). They find that CMIP5 models reproduce the spatial pattern of AOD  
87 reasonably well over eastern China, but with a tendency to underestimate AOD magnitudes (Liu and  
88 Liao, 2017; Park et al., 2014; Allen et al., 2013). GFDL-CM3 performs best among CMIP5 models in  
89 simulating AOD over eastern China, partly because it includes nitrate and ammonium that most models  
90 lack (Li et al., 2020). Other studies suggest that CMIP6 models simulate the magnitude of annual mean  
91 AOD better than CMIP5 over eastern China, in part due to the notable increase in sulfate (Cherian and  
92 Quaas, 2020; Fan et al., 2018a). Nonetheless, the CMIP6 models fail to capture the seasonal north-south  
93 shift of AOD maximum center over China during 2000–2014 (Li et al., 2021) and the observed dipole

94 pattern of AOD trends between China and India during 2006–2014 (Wang et al., 2021b).

95 Different PM<sub>2.5</sub> components exhibit distinctive radiative effects, thus understanding the performance of  
96 ESMS in simulating individual PM<sub>2.5</sub> components is important. Due to the absence of publicly available  
97 observational component data over China, only a few studies target single aerosol components (such as  
98 sulfate and dust) over a large region of the country, or different PM<sub>2.5</sub> components over a short period or  
99 a small region (Pu and Ginoux, 2018; Zhao et al., 2022). For example, model evaluation based on the  
100 Acid Deposition Monitoring Network in East Asia (EANET) suggests that sulfate concentrations  
101 simulated by CMIP5 and CMIP6 show a rising trend similar to observations (Mulcahy et al., 2020), but  
102 the simulations are still lower than observed concentrations (Fan et al., 2018b; Mortier et al., 2020). A  
103 recent study compares PM<sub>2.5</sub> components (dust, sea salt, BC, OC and sulfate) in CMIP6 models with the  
104 Modern Era Retrospective analysis for Research and Applications Aerosol Reanalysis (MERRAero) in  
105 Asia from 2005 to 2020 (Su et al., 2022; Buchard et al., 2016). The study shows that CMIP6 model  
106 uncertainties of total PM<sub>2.5</sub> over East Asia are mainly attributable to sulfate and mineral dust simulations.  
107 However, the model biases may in part come from other components (nitrate and ammonium) that are  
108 not analyzed in their study; and the MERRAero data might contain errors as well (Ma et al., 2021;  
109 Mahesh et al., 2019).

110 In this study, we evaluate near-surface concentrations of PM<sub>2.5</sub> and its five main components (OC, BC,  
111 sulfate, nitrate, and ammonium) from 2000 to 2014 over China simulated by fourteen CMIP6 models  
112 driven by historical emissions. For this purpose, we employ a satellite-based dataset for total PM<sub>2.5</sub>  
113 concentrations and a self-compiled PM<sub>2.5</sub> component dataset from 221 ground stations during 2000–2014  
114 collected from the literature. Section 2 introduces CMIP6 model simulations, satellite-based total PM<sub>2.5</sub>  
115 concentration data, and literature-based PM<sub>2.5</sub> component data. Section 3 assesses the performance of  
116 CMIP6 models for total PM<sub>2.5</sub>. Section 4 evaluates the simulated PM<sub>2.5</sub> components. Section 5 discusses  
117 the climate implications of the inadequacies in total PM<sub>2.5</sub> and its components in CMIP6 models. Section  
118 6 concludes the study.

119 **2 Data and method**

120 **2.1 CMIP6 simulations**

121 Near-surface concentrations of total PM<sub>2.5</sub> and its components can be converted from dry aerosol mass  
122 mixing ratios (MMRs) in CMIP6 models. Monthly mean near-surface MMRs (in the lowest model layer)  
123 of PM<sub>2.5</sub> and its main components are taken from fourteen CMIP6 models to assess the performance of  
124 ESMs over China (Table S1). Data are obtained from the “Historical” experiments covering 1850–2014,  
125 which serve as the entry cards for participating in CMIP6 (Eyring et al., 2016). They are coupled  
126 atmosphere-ocean simulations that include all CMIP6 historical forcings, and are well suited for  
127 quantifying and understanding model characteristics. The ensemble mean is taken for each model by  
128 averaging all available ensemble members. For GISS models, the ensemble members use two physics  
129 configurations with drastically different aerosol parameterizations. We average the ensemble members  
130 using the same physics configurations in GISS models, named GISS-E2-1-OMA (physics-version = 3)  
131 and GISS-E2-1-MATRIX (physics-version = 5) respectively (Bauer et al., 2020). Simulation results over  
132 2000–2014 are selected and re-gridded to 1° × 1° for comparison with available satellite- and ground-  
133 based data.

134 The anthropogenic emission data (ver. 2016-07-26) to drive “Historical” CMIP6 simulations is produced  
135 by the Community Emissions Data System (CEDS) (Hoesly et al., 2018). An updated version of CEDS  
136 (ver. 2017-05-18) corrected several errors in the spatial distribution within each country, but does not  
137 change total emissions by country and sector (Feng et al., 2020). The CEDS emissions (ver. 2016-07-26  
138 and ver. 2017-05-18) of OC, BC, CO, NO<sub>x</sub> and SO<sub>2</sub> in China after 2000 are higher than those in the  
139 Multi-resolution Emission Inventory for China (i.e., MEIC) (Paulot et al., 2018; Zheng et al., 2018) and  
140 the Peking University (PKU) inventory (Wang et al., 2014; Huang et al., 2015; Tao et al., 2018) which  
141 use more detailed Chinese data. This difference in China has been reduced when CEDS was used to  
142 derive future SSP scenarios in CMIP6 simulations (published on ESGF on 28 June 2018 on [https://esgf-](https://esgf-node.llnl.gov/search/cmip6)  
143 [node.llnl.gov/search/cmip6](https://esgf-node.llnl.gov/search/cmip6)), and has been included in a post-CMIP6 version of CEDS (McDuffie et al.,  
144 2020).

145 Of the fourteen models, all output the MMRs of OA, BC, sulfate, dust and sea salt, five output ammonium,  
146 and four output nitrate (Table S1). Seven models output the MMRs of total PM<sub>2.5</sub>, as the sum over all

147 components with suitable particle sizes. The MMRs are converted to mass concentrations ( $\mu\text{g m}^{-3}$ ) based  
148 on air density in each model. In evaluating  $\text{PM}_{2.5}$  components (Sect. 4), the evaluation of dust and sea  
149 salt concentrations is excluded due to the lack of available ground-based observations. We compare OC,  
150 BC, sulfate, nitrate, and ammonium simulations with the observed data available for these components.  
151 Modeled OA is converted to organic carbon (OC) to be comparable with the observational dataset.  
152 Modeled OA refers to total organic aerosol, including primary organic aerosol (POA) and secondary  
153 organic aerosol (SOA). For the GFDL-ESM4 model, the “mmroa” variable for OA only includes POA;  
154 thus we calculate the total OA of GFDL-ESM4 as mmroa plus mmrsoa. The OA/OC ratios in the  
155 literature range from 1.4 to 2.1 (Bürki et al., 2020; Lin et al., 2016). We choose an OA/OC ratio of 1.6,  
156 which is the same as the ratio used in converting near-surface OA observations to OC. This ratio is  
157 slightly higher than the value of 1.4 recommended by CMIP6 for POA, but it does not affect the relative  
158 (percentage) model bias found in this study because the same ratio is used for models and observations.

159 For the seven models that do not output total  $\text{PM}_{2.5}$ , we follow the previous work to estimate total  $\text{PM}_{2.5}$   
160 concentrations (Eq. 1) (Turnock et al., 2020). Here, OA, BC, sulfate and certain portions of sea salt (SSLT,  
161  $a_1$ ) and dust (DST,  $a_2$ ) are assumed to be present in fine particles (diameter  $< 2.5 \mu\text{m}$ ).

$$162 \quad \text{PM}_{2.5} = \text{OA} + \text{BC} + \text{SO}_4^{2-} + a_1 \times \text{SSLT} + a_2 \times \text{DST} \quad (1)$$

163 For most models, specific values of  $a_1$  and  $a_2$  are provided by model developers (Table S2). BCC-ESM1  
164 does not provide the coefficients. Instead, the model outputs concentrations in four size bins for each of  
165 dust (DST01: 0.1–1.0  $\mu\text{m}$ , DST02: 1.0–2.5  $\mu\text{m}$ , DST03: 2.5–5.0  $\mu\text{m}$ , and DST04: 5.0–10  $\mu\text{m}$ ) and sea  
166 salt (SSLT01: 0.2–1.0  $\mu\text{m}$ , SSLT02: 1.0–3.0  $\mu\text{m}$ , SSLT03: 3.0–10  $\mu\text{m}$ , and SSLT04: 10–20  $\mu\text{m}$ ) (Su et  
167 al., 2022; Wu et al., 2019). Thus, the first two bins are assumed to belong to  $\text{PM}_{2.5}$ . Ammonium and  
168 nitrate are not available in most of these six models (except GISS-E2-1-MATRIX) and are thus not  
169 included in Eq. 1.

## 170 **2.2 Satellite-based total $\text{PM}_{2.5}$**

171 We take satellite-based near-surface total  $\text{PM}_{2.5}$  concentrations from the V4.CH.03 product of the  
172 Washington University Atmospheric Composition Analysis Group (Hammer et al., 2020). The dataset is  
173 constructed by combining multiple satellite products of AOD with simulations from a chemical transport

174 model (GEOS-Chem) to predict PM<sub>2.5</sub>, and then constraining these estimates by ground-level PM<sub>2.5</sub>  
175 monitoring. The GEOS-Chem aerosol simulations include primary and secondary carbonaceous aerosols,  
176 sulfate, nitrate, ammonium, mineral dust, and sea salt. The dataset provides the annual average PM<sub>2.5</sub>  
177 concentrations during the period 2000–2014 with a high spatial resolution of 0.01° × 0.01° (~1 × 1 km<sup>2</sup>).  
178 The adjusted satellite-derived PM<sub>2.5</sub> concentrations over Asia are compared with surface PM<sub>2.5</sub>  
179 observations collected from the Global Burden of Disease (GBD) collaborators during the period 2008–  
180 2013 (Mean<sub>satellite</sub> = 61.5 μg m<sup>-3</sup> versus Mean<sub>obs</sub> = 59.1 μg m<sup>-3</sup>) (van Donkelaar et al., 2016) and from the  
181 China National Environmental Monitoring Center (CNEMC) during the period 2015–2019 (Mean<sub>satellite</sub>  
182 = 45.9 μg m<sup>-3</sup> versus Mean<sub>obs</sub> = 43.4 μg m<sup>-3</sup>) (van Donkelaar et al., 2021). Detailed data descriptions are  
183 provided elsewhere (van Donkelaar et al., 2019; van Donkelaar et al., 2016). Here the satellite-based  
184 total PM<sub>2.5</sub> data are re-gridded to 1° × 1° for model evaluation purposes.

### 185 **2.3 Ground-based PM<sub>2.5</sub> components data**

186 Since national-scale continuous measurements of near-surface PM<sub>2.5</sub> components are unavailable in  
187 China, we collect observational PM<sub>2.5</sub> component data from the literature. Our collected dataset includes  
188 2469 component records of OC, BC, sulfate, nitrate, and ammonium nationwide (627, 66, 645, and 1131  
189 records in western regions, Northeast China, North China, and Central and South China, respectively),  
190 as shown in Figure 1. Here a record represents one measured PM<sub>2.5</sub> component at the specific sample site  
191 and period. These records cover 30 provinces (including provinces and provincial-level municipalities)  
192 and multiple land use types (urban, rural, near the road, and industrial park, etc.). The dataset does not  
193 cover Ningxia, Guizhou, Heilongjiang, and Taiwan. A total of 472, 459, 518, 519, and 501 records are  
194 available for OC, BC, sulfate, nitrate, and ammonium over China, respectively. The site locations,  
195 sampling periods, data sources, and other information are summarized in the Supplement.

196 At a given site, the records are not continuous in time. These records cover varying sampling periods  
197 ranging from a few days to several years, although most are monthly data. We treat a record as seasonal  
198 if its data length is equal to or shorter than a season, or as annual when its data length is longer than 6  
199 months. The records are not evenly scattered across years and are more available in later years in general.  
200 From 2000 to 2008, the numbers of records range from 50 to 150 per year, except for 2003 (207 records);  
201 while from 2009 to 2014, the numbers of records vary between 150 to 550 per year (Fig. S1). To compare

202 with CMIP6 simulations, we calculate for each site the multi-year mean  $\text{PM}_{2.5}$  component concentrations  
203 by averaging over the seasonal or annual observational records. If there are more than one sites in a given  
204 model grid cell, we average data from all sites in that grid cell. To consider the effect of interannual  
205 variability (caused by incomplete temporal match in data availability between models and observations),  
206 we compute for each CMIP6 model the average and maximum of annual mean values during 2000–2014  
207 from all grid cells with available observational data, and then compare with the multi-year averaged  
208 observations from these grid cells. As detailed in Section 5, the model biases are not caused by imperfect  
209 model-observation matching in time.

### 210 **3 Evaluation of near-surface total $\text{PM}_{2.5}$**

#### 211 **3.1 Spatial distribution**

212 The spatial distribution of satellite-based annual mean total  $\text{PM}_{2.5}$  concentrations (Fig. 2 p) exhibits high  
213 values over populous and industrial North China (including Beijing, Tianjin, Hebei, Shandong, and  
214 Shanxi provinces,  $52.6 \mu\text{g m}^{-3}$ ) and eastern Sichuan ( $60.9 \mu\text{g m}^{-3}$ ). Central and South China exhibits  
215  $\text{PM}_{2.5}$  concentrations ( $46.5 \mu\text{g m}^{-3}$ ) lower than North China, due to lower emissions, higher vegetation  
216 coverage, better ventilation conditions and more precipitation.  $\text{PM}_{2.5}$  concentrations are modest over  
217 dusty southern Xinjiang ( $33.6 \mu\text{g m}^{-3}$ ). Low  $\text{PM}_{2.5}$  concentrations ( $< 8 \mu\text{g m}^{-3}$ ) are distributed over the  
218 plateaus or forested regions with small populations, such as Tibet and northern Heilongjiang. Overall,  
219  $\text{PM}_{2.5}$  concentrations in the south and coastal regions are lower than in the northern and inland regions.

220 Among the seven models that directly output total  $\text{PM}_{2.5}$  concentrations (Fig. 2 a-g), GFDL-ESM4 and  
221 MPI-ESM1-2-HAM show similar patterns and magnitudes to satellite data with small national average  
222 biases ( $-1.5\%$  and  $-1.1\%$ , respectively) because of better performance in BC, sulfate, and ammonium  
223 simulations (Fig. S4-S7), which are related to the aerosol-chemistry-climate schemes within CMIP6  
224 models (Turnock et al., 2020). Over the eastern regions (including Northeast China, North China, and  
225 Central and South China), all models exhibit spatially averaged negative biases ranging from by  $-47.9\%$   
226 to  $-3.3\%$  (Fig. S2). Nevertheless, the spatial pattern over the eastern regions is well simulated by four  
227 models (GFDL-ESM4, GISS-E2-1-OMA, MIROC-ES2L, and MPI-ESM1-2-HAM) ( $R > 0.9$ , as shown  
228 in Table S2) with the maximum center over North China correctly reproduced. Over the western regions,  
229 four models (GFDL-ESM4, MRI-ESM2-0, NorESM2-LM, and NorESM2-MM) reproduce the



230 maximum center over southern Xinjiang, although each of the seven models can underestimate or  
231 overestimate the peak values substantially.

232 For the seven models with total  $PM_{2.5}$  derived from Eq.1, their simulated  $PM_{2.5}$  concentrations  
233 underestimate the satellite-based data by  $-65.5\%$  to  $-48.0\%$  averaged over the country (Fig.2 h-n). The  
234 negative biases are in part because nitrate and ammonium are not included. About  $15.1\text{--}20.6\%$  and  $11.4\text{--}$   
235  $14.6\%$  of  $PM_{2.5}$  are nitrate and ammonium in the models that do contain them, as shown in Table S3.  
236 Over the eastern regions, HadGEM3-GC31-LL and UKESM1-0-LL exhibit the least underestimation,  
237 and they also capture the observed maximum center over North China. Five of these seven models do  
238 not reproduce the  $PM_{2.5}$  peaks over dusty regions in the west, pointing to model deficiencies in dust  
239 simulations (Zhao et al., 2022).

### 240 **3.2 Trend and interannual variability**

241 Over the eastern regions (Northeast China, North China, and Central and South China), data from satellite  
242 ( $0.72 \mu\text{g m}^{-3} \text{yr}^{-1}$ ) and all models ( $0.32\text{--}1.14 \mu\text{g m}^{-3} \text{yr}^{-1}$ ) exhibit significant increases ( $p\text{-value} < 0.05$ )  
243 in annual mean total  $PM_{2.5}$  concentrations over 2000–2014, with temporal correlation between 0.63 and  
244 0.87 (Fig. 3 a and Table S2). The positive trend of satellite data over the eastern regions is consistent  
245 with findings from previous studies (de Leeuw et al., 2022; Geng et al., 2021) , as caused mainly by  
246 emission changes (Hoesly et al., 2018; Wang et al., 2022). GFDL-ESM4 and MPI-ESM1-2-HAM exhibit  
247 annual average  $PM_{2.5}$  concentrations and trends similar to the satellite data since 2004. Regionally, the  
248 fourteen models capture the interannual variations of satellite  $PM_{2.5}$  over Northeast China ( $R > 0.9$ ) and  
249 North China ( $R > 0.8$ ) (Fig. 4). The temporal consistency reflects that the models capture the temporal  
250 changes in anthropogenic emissions over these polluted regions, although the models might not align  
251 with natural (meteorology-driven) variability.

252 Over the western regions where natural dust dominates the aerosol loadings, satellite-based  $PM_{2.5}$   
253 concentrations experience no significant trend over 2000–2014, whereas 11 models increase significantly  
254 ranging from  $0.10\text{--}0.28 \mu\text{g m}^{-3} \text{yr}^{-1}$ ) (Fig. 3 b). There is a notable decline over 2000–2005 in satellite  
255 data ( $-1.12 \mu\text{g m}^{-3} \text{yr}^{-1}$ , at the significance level of 0.1) consistent with the previous studies that use dust  
256 aerosol optical depth (DOD) and ground-based observations of dust storm (Wang et al., 2021a; Song et

257 al., 2016). However, the dramatic drop is not captured by any model, reflecting large uncertainties and  
258 inter-model diversities in dust simulations stemming from many factors such as the driving mechanisms,  
259 dust particle size, and model structural differences (Zhao et al., 2022). Over 2000–2014, NorESM2-LM,  
260 NorESM2-MM, and MPI-ESM-1-2-HAM show large interannual variations whereas other models do  
261 not. The models do not align with the yearly changes found in the satellite data, with modestly positive,  
262 low or even negative correlation coefficients (–0.6 to 0.6, Fig. 4). The inaccuracy in aerosol trend and  
263 variability might exert erroneous forcing upon the climate system.

## 264 **4 Evaluation of near-surface PM<sub>2.5</sub> components**

### 265 **4.1 Organic carbon and black carbon**

266 Ground-based observations of carbonaceous aerosols (OC and BC) are mostly available in the eastern  
267 regions. The national average multi-year mean observed OC concentration reaches  $15.9 \mu\text{g m}^{-3}$ .  
268 Observed OC concentrations peak over North China ( $> 25 \mu\text{g m}^{-3}$ ) and are also high over Central and  
269 South China ( $5\text{--}25 \mu\text{g m}^{-3}$ ) (Fig. 5 a). The national average of the 14-model mean ( $6.5 \mu\text{g m}^{-3}$ , normalized  
270 mean bias (NMB) =  $-59.0\%$ ), which is spatially coincidently sampled with the ground-based  
271 observations (i.e., model values are obtained from grid cells with available observations), severely  
272 underestimates the observations, especially over parts of North China with the bias reaching  $-40 \mu\text{g m}^{-3}$   
273 (Fig. 5 b). Nevertheless, the spatial pattern of OC observations is captured by the 14-model mean  
274 modestly well with a correlation coefficient of 0.51. Further, a negative bias exceeding  $-50\%$  occurs in  
275 11 models, even though they can simulate the spatial pattern moderately well (R ranges from 0.40 to  
276 0.58, Fig. S4).

277 The national average multi-year mean observed BC concentration is  $4.3 \mu\text{g m}^{-3}$ . Observed BC  
278 concentrations are high ( $> 10 \mu\text{g m}^{-3}$ ) over parts of North China with mining and other heavy industries,  
279 such as Hebei and Shanxi province (Fig. 5 d). However, the 14-model mean ( $3 \mu\text{g m}^{-3}$ ) does not capture  
280 the spatial pattern very well (R = 0.39) and it underestimates the observations (NMB =  $-27.2\%$ ). The 14-  
281 model mean presents the largest negative bias over Shanxi ( $-15.2 \mu\text{g m}^{-3}$ ) and the greatest positive bias  
282 over Shandong ( $3.9 \mu\text{g m}^{-3}$ , Fig. 5 e); both provinces are in North China. Twelve of the 14 models  
283 underestimate the BC observations (by  $-47.9\%$  to  $-12.1\%$  for national average), whereas two models  
284 (HadGEM3-GC31-LL and UKESM1-0-LL) exhibit positive biases (by 21.1% and 26.2%, respectively)

285 (Fig. 6 and Fig. S5). Most models produce high concentrations of BC over the whole North China,  
286 including Beijing and Shandong that exhibit relatively low observational values. The spatial distributions  
287 of carbonaceous aerosol concentrations are mainly influenced by CEDS emissions used in models, with  
288 higher spatial correlation coefficients greater than 0.85 (Fig. S3).

289 The underestimation of carbonaceous aerosol concentrations might be associated with anthropogenic  
290 emissions, chemical mechanisms, and meteorological conditions. For China, the CEDS emission data  
291 (ver. 2016-07-26) used in CMIP6 historical simulations are about 3.8–31.3% higher than those in MEIC  
292 inventory except for NO<sub>x</sub> emissions (Fan et al., 2022). However, the positive bias in emissions cannot  
293 explain the model underestimation of OC and BC concentrations. The model inadequacies in chemical  
294 processes (e.g., using simplified aerosols and chemistry schemes, which tends to underestimate aerosol  
295 formation (Turnock et al., 2020)) might lead to underestimated secondary organic aerosols (SOA, as a  
296 component of OC), especially over Central and South China (Chen et al., 2016). The inter-model  
297 discrepancies of OC and BC peak over North China and eastern Sichuan (Fig. 5 c). The large absolute  
298 discrepancies are in part due to the higher air pollutant concentrations in these regions. Furthermore,  
299 many differences exist among CMIP6 models in PM<sub>2.5</sub> component simulations, including the  
300 representation of aerosol size distribution; the simplification of chemical processes with photolytic,  
301 kinetic and heterogeneous reactions (e.g., 33 photolytic reactions in BCC-ESM1 but 43 in GFDL-ESM4)  
302 (Turnock et al., 2020; Wu et al., 2020b; Dunne et al., 2020); the treatment for transport of gaseous tracers  
303 and aerosols by advection and vertical convection; and the dry deposition and wet scavenging schemes  
304 (Su et al., 2022; Digby et al., 2024).

305 Meteorological conditions, including temperature, precipitation and surface wind simulations, have  
306 critical impacts on local aerosol concentrations. Temperature simulations over the eastern regions of  
307 China by CMIP6 models are very close to the observed data (Yang et al., 2021). Over the western regions,  
308 a notable warm bias over Xinjiang in most CMIP6 models (Zhang et al., 2022b) may contribute to higher  
309 planetary boundary layer height (Yue et al., 2021) and stronger vertical mixing, partly explaining the  
310 underestimation of OC and BC concentrations near the surface (Fig. 5); whereas the pronounced cold  
311 bias over the Tibetan Plateau (Zhu and Yang, 2020) might contribute to overestimated near-surface  
312 aerosol concentrations over there. Precipitation affects aerosol concentrations through wet scavenging;

313 and it is overestimated (wet bias) in CMIP6 models over North China and Northeast China but close to  
314 observations over Central and South China (Yang et al., 2021). The model performance in precipitation  
315 may partly explain the more severe underestimation of OC concentrations over North China than over  
316 Central and South China. But the overestimation of BC over North China suggests that other factors  
317 offset the influence of local wet bias. Over the western regions, most models exhibit wet bias, except  
318 over northern Xinjiang where local temperature (warm bias) and precipitation (dry bias) have opposite  
319 effects on near-surface aerosol concentrations. Furthermore, the overall underestimation of surface wind  
320 speed over China in CMIP6 (Wu et al., 2020a) is conducive to the accumulation of near-surface aerosol  
321 concentrations around the anthropogenic emission source regions, which may induce a negative  
322 contribution to the underestimation of OC and BC concentrations.

#### 323 **4.2 Sulfate, nitrate and ammonium**

324 This section evaluates the model performance of secondary inorganic aerosols (sulfate, nitrate, and  
325 ammonium; SIOA). Sulfate aerosol in CMIP6 models is dependent on SO<sub>2</sub> emissions (the main sulfuric  
326 acid precursor), chemical conversion of SO<sub>2</sub> to sulfate, and loss through wet scavenging (Wu et al., 2020b;  
327 Tegen et al., 2019). Some models also explicitly simulate nitrate and ammonium aerosols using the  
328 sulfate-nitrate-ammonia thermodynamic equilibrium. For instance, EC-Earth3-AerChem, GISS-E2-1-  
329 MATRAX and GISS-E2-1-OMA use the Equilibrium Simplified Aerosol Model (EQSAM) (Metzger et  
330 al., 2002; Bauer et al., 2020; van Noije et al., 2021), while GFDL-ESM4 treats ammonium and nitrate  
331 aerosols with ISORROPIA (Fountoukis and Nenes, 2007; Paulot et al., 2016; Dunne et al., 2020).

332 The national average multi-year mean of observed sulfate concentrations reaches 14.6  $\mu\text{g m}^{-3}$ , the second  
333 largest value among the five PM<sub>2.5</sub> components (following OC). The observed sulfate concentrations  
334 exceed 15  $\mu\text{g m}^{-3}$  over most of North China and eastern Sichuan, as well as cities over Xinjiang with  
335 large population and petroleum industry (Fig. 5 g). The 14-model mean, whose national average is 9.3  
336  $\mu\text{g m}^{-3}$ , has the greatest underestimation over North China and Xinjiang (Fig. 5 h). The 14-model mean  
337 agrees modestly well with the observations in spatial pattern ( $R = 0.57$ ). Among the 14 models, the  
338 national average model biases range from -66.1% (GISS-E2-1-OMA) to 24.5% (MRI-ESM2-0); and  
339 five models better capture the observed spatial pattern with correlation coefficients exceeding 0.6 (Fig.  
340 6). The cross-model discrepancy in sulfate (2  $\mu\text{g m}^{-3}$  in national average) is larger than those for the other

341 four components ( $0.4\text{--}0.9\ \mu\text{g m}^{-3}$ ), particularly over Central and South China (Fig. 5 i).

342 The national average multi-year mean of observational nitrate concentrations is  $8.7\ \mu\text{g m}^{-3}$ . The observed  
343 spatial pattern of nitrate is similar to sulfate, with high values over North China, eastern Sichuan and  
344 populous cities of Xinjiang (Fig. 5 j). Only four models (GFDL-ESM4, GISS-E2-1-OMA, GISS-E2-1-  
345 MATRIX, and EC-Earth3-AerChem) include nitrate simulations. The 4-model mean has a national  
346 average of  $5.5\ \mu\text{g m}^{-3}$ , with a NMB of  $-36.5\%$ ; but it captures the observed spatial pattern very well with  
347 a correlation coefficient reaching 0.7. All the four models exhibit negative NMBs ranging from  $-41.4\%$   
348 to  $-25.4\%$ ; they reproduce high values over the eastern regions but have underestimation over Xinjiang  
349 (Fig. S7).

350 The observed multi-year mean ammonium concentrations have a national average value of  $6.7\ \mu\text{g m}^{-3}$ .  
351 The observational values peak over North China ( $> 10\ \mu\text{g m}^{-3}$ ), particularly over the agricultural regions  
352 from which ammonia emissions are the greatest (Fig. 5 m). Five models perform ammonium simulations.  
353 The 5-model mean, with a national average of  $3.4\ \mu\text{g m}^{-3}$ , has negative and positive biases between  $-$   
354  $12.2$  and  $1.5\ \mu\text{g m}^{-3}$  at different locations (Fig. 5 n). The 5-model mean captures the observed spatial  
355 pattern of ammonium ( $R = 0.74$ ) better than for other components ( $R = 0.39\text{--}0.70$ ). The five models  
356 exhibit varying performances in magnitude and spatial pattern. The NMBs range from  $-89.0\%$  to  $-13.6\%$   
357 across these models. Four models simulate the spatial patterns of ammonium well with high correlation  
358 coefficients between 0.67 to 0.76, although the spatial agreement is poor for CESM2-WACCM ( $R =$   
359 0.21).

360 Emissions, meteorological conditions and chemical processes affect the formation and loss of secondary  
361 inorganic aerosols. As explained in Sect. 4.1, the potentially overestimated CEDS emissions over China,  
362 the cold bias over the Tibetan Plateau, and the dry bias over northern Xinjiang tend to overestimate  
363 aerosol concentrations, which are in contrast with the negative model biases over the respective regions.  
364 On the other hand, the warm bias over northern Xinjiang and the wet bias over North China and Northeast  
365 China are in line with the underestimation of aerosol concentrations. Furthermore, the formation of  
366 nitrate from nitric acid depends on the amount of residual ammonia left from the formation of ammonium  
367 sulfate. Over the regions where ammonia is not sufficient to neutralize both nitric acid and sulfuric acid  
368 (such as Shanxi and Shandong), decreased sulfate formation might promote nitrate formation with the

369 released ammonium (Zhai et al., 2019; Zhai et al., 2021). This partly explains why the underestimation  
370 of nitrate simulations is less than sulfate over these regions.

## 371 **5 Discussion**

372 Over the eastern regions, the concentrations of total  $PM_{2.5}$  and its five components are underestimated  
373 by the 14 models in general. The slight underestimation of three models (GFDL-ESM4, MPI-ESM-1-2-  
374 HAM, and MRI-ESM2-0) can be traced to positive biases in sulfate simulations partly offsetting the  
375 negative biases in OC and BC. Over the western regions, most models underestimate the total  $PM_{2.5}$   
376 concentrations dominated by dust aerosols, whereas three models (GFDL-ESM4, NorESM2-LM, and  
377 NorESM2-MM) produce overly high values over Xinjiang due to overestimated dust concentrations.  
378 Meanwhile, all models underestimate the five  $PM_{2.5}$  components over the west.

379 Figure 7 shows little difference between the maximum and average annual concentrations over 2000–  
380 2014 for national mean  $PM_{2.5}$  components simulated by individual models. Furthermore, we average  
381 over all seasonal and annual observational records to compare with annual mean model results. A test  
382 using the seasonal (annual) model results to match seasonal (annual) observational records shows very  
383 similar comparison results (Fig. S8). These tests suggest that the model underestimation cannot be  
384 attributed to imperfect temporal matching between models and observations or the potential mis-phase  
385 (or variability) in models.

386 Among the five  $PM_{2.5}$  components evaluated, absorbing aerosol (BC) and four scattering aerosols (OC,  
387 sulfate, nitrate, and ammonium) have opposite direct radiative forcing at the top of atmosphere (TOA).  
388 The underestimation of BC is less than for the other four scattering aerosols. If this difference persists in  
389 the troposphere, the underestimated  $PM_{2.5}$  components might cause an underestimation of negative  
390 radiative forcing at TOA. The underestimation of BC and scatter aerosols might result in more solar  
391 radiation reaching the ground (Chen et al., 2022; Tang et al., 2022). This is consistent with the  
392 overestimation of maximum daily maximum temperature over the eastern regions (Zhu et al., 2020),  
393 likely serving as a positive feedback between negative aerosol biases and overestimated surface  
394 temperature.

395 The spatial biases in aerosols might also serve as an important limiting factor for the performance of

396 meteorological/climate simulations. The observed PM<sub>2.5</sub> and its five components are characterized by  
397 high concentrations over the east and low values over the west (except northern Xinjiang). In a few  
398 models, the large overestimation of PM<sub>2.5</sub> over Xinjiang of the west (dominated by dust) with  
399 underestimated PM<sub>2.5</sub> (dominated by anthropogenic aerosols) over the east might exert an incorrect west-  
400 east asymmetric climate forcing. The spatial pattern of resulting climate response might include cold-  
401 warm biases of surface temperature (cold bias over the west and warm bias over the east). The difference  
402 in the spatial pattern of model bias between BC and scattering aerosols might have additional impacts on  
403 the climate. Future work is needed to examine how the model errors in PM<sub>2.5</sub> and its components might  
404 affect climate simulations through aerosol-climate feedback.

## 405 **6 Summary**

406 In this study, we evaluate the performance of 14 CMIP6 ESMs in simulating total near-surface PM<sub>2.5</sub> and  
407 its five components over China during 2000–2014, and discuss the likely causes for model errors, and  
408 their climate implications. Our assessment helps to understand the capability of the current-generation  
409 models in the simulation of aerosols and aerosol-climate interactions, towards further improvement of  
410 climate predictions and projections. Our findings are summarized as follows:

411 (1) Twelve of the 14 CMIP6 models tend to underestimate the total PM<sub>2.5</sub> concentrations over China  
412 (NMB = –65.5% to –1.1%) and the other two models overestimate them (NMB = 17.0%–39.2%), as  
413 compared to a satellite-based dataset. The seven models that output total PM<sub>2.5</sub> concentrations exhibit  
414 underestimation between –47.9% and –3.3% over the eastern regions, although four of them capture the  
415 observed spatial pattern ( $R > 0.9$ ). Over the western regions, four of these seven models reproduce the  
416 maximum center over southern Xinjiang. The seven models, for which we calculate the total PM<sub>2.5</sub>  
417 concentrations from outputted components, underestimate the observed PM<sub>2.5</sub> by –65.5% to –48.0%  
418 averaged over the country, in part due to missing nitrate and ammonium in the models.

419 (2) Over the eastern regions, all models simulate significant increasing trends of total PM<sub>2.5</sub> (0.32–1.14  
420  $\mu\text{g m}^{-3} \text{ yr}^{-1}$ ) over 2000–2014 that are close to satellite-based data (0.72  $\mu\text{g m}^{-3} \text{ yr}^{-1}$ ). The models also  
421 capture the interannual variability of satellite PM<sub>2.5</sub> over Northeast China and North China. Over the  
422 western regions, 11 models simulate growing PM<sub>2.5</sub> concentrations at rates of 0.10–0.28  $\mu\text{g m}^{-3} \text{ yr}^{-1}$ , in

423 contrast to no significant trends in satellite data.

424 (3) The 14-model mean captures the spatial pattern of observed OC modestly well ( $R = 0.51$ ), but it  
425 exhibits severe underestimation nationwide ( $NMB = -59.0\%$ ), with negative biases exceeding  $-50\%$  in  
426 11 models. The 14-model mean shows a poor capability in capturing the BC spatial pattern ( $R = 0.39$ ),  
427 and it also underestimates the BC observations ( $NMB = -27.2\%$ ). Two models exhibit positive biases in  
428 BC, while the other 12 models exhibit negative biases.

429 (4) Fourteen, four and five models output the sulfate, nitrate, and ammonium, respectively. The 14-  
430 model mean of sulfate exhibits modest spatial correlation and bias ( $R = 0.57$ ,  $NMB = -36.5\%$ ); and there  
431 exist large discrepancies among these models, with biases ranging from  $-66.1\%$  to  $24.5\%$ . The 4-model  
432 mean of nitrate captures the spatial pattern well ( $R = 0.7$ ), although it still underestimates concentrations  
433 nationwide ( $NMB = -36.5\%$ ). The 5-model mean of ammonium has the best performance in reproducing  
434 the spatial pattern ( $R = 0.74$ ) but with a negative bias in magnitudes ( $NMB = -46.5\%$ ).

435 (5) The overall underestimation of  $PM_{2.5}$  and its components are associated with imperfectness in  
436 emissions as input, modeled meteorology and chemistry. The underestimated  $PM_{2.5}$  and its components  
437 might cause an overall underestimated cooling effect at TOA and stronger warming at the surface in the  
438 models. The model performance in spatial pattern differs between BC and scattering aerosols; and a few  
439 models also exhibit strong positive biases over the west (associated with dust) but negative biases over  
440 the east. Together, the errors in spatial pattern might have additional consequences for the modeled  
441 climate. Further studies are warranted to quantify how model errors in the magnitude and spatial pattern  
442 of aerosols affect the regional and global climate, for example, through the Regional Aerosol Model  
443 Intercomparison Project (RAMIP) (Wilcox et al., 2022).

444 As a final note, those causes for aerosol underestimation may also affect ozone, and the underestimated  
445 aerosol concentrations might also further affect the ozone simulation through radiative or heterogeneous  
446 chemical processes (Jacob, 2000; Lin et al., 2012; Li et al., 2019). In addition, as CMIP6 models are also  
447 used to study the health impacts of aerosols (Xu et al., 2022; Shim et al., 2021), the aerosol  
448 underestimation needs to be corrected to allow a more reliable estimate of health consequences.



449 **Data availability**

450 CMIP6 data are available on the Earth System Grid Federation (ESGF) and can be freely downloaded  
451 via the website interface <https://esgf-data.dkrz.de/search/cmip6-dkrz/> (last access: 8 September 2020,  
452 WCRP, 2020). Satellite-derived surface PM<sub>2.5</sub> concentration products can be accessed from the  
453 Washington University Atmospheric Composition Analysis Group website as version V4.CH.03 at  
454 <https://sites.wustl.edu/acag/datasets/surface-pm2-5/>. Observational data used in this paper are provided  
455 in the SI, with raw data available upon request to the corresponding author Jintai Lin (linjt@pku.edu.cn).

456 **Author contributions**

457 JL led the study. FR and JL designed the study, analyzed the results, and wrote the paper. CX provided  
458 the map data of four regions in China. JA collected observation data of PM<sub>2.5</sub> components from the  
459 literature. JW helped to analyze the evaluation results. RM, AD and MH provided satellite-derived data  
460 of total PM<sub>2.5</sub>. ST performed UKESM1-0-LL and HadGEM3-GC31-LL simulations. NO performed  
461 MRI-ESM2-0 simulations. JZ performed BCC-ESM1 simulations. SB and KT performed GISS-E2-1-  
462 OMA and GISS-E2-1-MATRIX simulations. ØS performed NorESM2-LM and NorESM2-MM  
463 simulations. PN performed CNRM-ESM2-1 simulations. DN performed MPI-ESM1-2-HAM  
464 simulations. GS performed CESM2-WACCM simulations. TN and PS performed EC-Earth3-AerChem  
465 simulations. LH performed GFDL-ESM4 simulations. TT performed MIROC-ES2L simulations. All  
466 authors commented on the manuscript.

467 **Competing interests**

468 The authors declare that they have no conflict of interests.

469 **Financial support**

470 Jintai Lin and Fangxuan Ren have been supported by the National Natural Science Foundation of China  
471 (grant no. 42075175) and the second Tibetan Plateau Scientific Expedition and Research Program 525  
472 (grant no. 2019QZKK0604). Naga Oshima has been supported by the Environment Research and  
473 Technology Development Fund (grant nos. JPMEERF20202003 and JPMEERF20232001) of the  
474 Environmental Restoration and Conservation Agency provided by Ministry of the Environment of Japan,  
475 the Arctic Challenge for Sustainability II (ArCS II, grant no. JPMXD1420318865), and the Global

476 Environmental Research Coordination System from Ministry of the Environment, Japan (grant no.  
477 MLIT2253). David Neubauer has been supported by the European Union's Horizon 2020 research and  
478 innovation programme project (FORCeS, grant no. 821205). Randall Martin has been supported by  
479 NASA (grant no. 80NSSC21K0508).

## 480 **Reference**

481 Allen, R. J. and Landuyt, W.: The vertical distribution of black carbon in CMIP5 models: Comparison to  
482 observations and the importance of convective transport, *J. Geophys. Res. Atmos.*, 119, 4808-4835,  
483 <https://doi.org/10.1002/2014JD021595>, 2014.

484 Allen, R. J., Norris, J. R., and Wild, M.: Evaluation of multidecadal variability in CMIP5 surface solar  
485 radiation and inferred underestimation of aerosol direct effects over Europe, China, Japan, and India, *J.*  
486 *Geophys. Res. Atmos.*, 118, 6311-6336, <https://doi.org/10.1002/jgrd.50426>, 2013.

487 Bauer, S. E., Tsigaridis, K., Faluvegi, G., Kelley, M., Lo, K. K., Miller, R. L., Nazarenko, L., Schmidt,  
488 G. A., and Wu, J.: Historical (1850–2014) Aerosol Evolution and Role on Climate Forcing Using the  
489 GISS ModelE2.1 Contribution to CMIP6, *J. Adv. Model. Earth Syst.*, 12, e2019MS001978,  
490 <https://doi.org/10.1029/2019MS001978>, 2020.

491 Buchard, V., da Silva, A. M., Randles, C. A., Colarco, P., Ferrare, R., Hair, J., Hostetler, C., Tackett, J.,  
492 and Winker, D.: Evaluation of the surface PM<sub>2.5</sub> in Version 1 of the NASA MERRA Aerosol Reanalysis  
493 over the United States, *Atmos. Environ.*, 125, 100-111, <https://doi.org/10.1016/j.atmosenv.2015.11.004>,  
494 2016.

495 Bürki, C., Reggente, M., Dillner, A. M., Hand, J. L., Shaw, S. L., and Takahama, S.: Analysis of  
496 functional groups in atmospheric aerosols by infrared spectroscopy: method development for  
497 probabilistic modeling of organic carbon and organic matter concentrations, *Atmos. Meas. Tech.*, 13,  
498 1517-1538, <https://doi.org/10.5194/amt-13-1517-2020>, 2020.

499 Carslaw, K. S., Lee, L. A., Reddington, C. L., Pringle, K. J., Rap, A., Forster, P. M., Mann, G. W.,  
500 Spracklen, D. V., Woodhouse, M. T., Regayre, L. A., and Pierce, J. R.: Large contribution of natural  
501 aerosols to uncertainty in indirect forcing, *Nature*, 503, 67-71, <https://doi.org/10.1038/nature12674>, 2013.

502 Chen, D., Liao, H., Yang, Y., Chen, L., Zhao, D., and Ding, D.: Simulated impacts of vertical distributions  
503 of black carbon aerosol on meteorology and PM<sub>2.5</sub> concentrations in Beijing during severe haze events,  
504 *Atmos. Chem. Phys.*, 22, 1825-1844, <https://doi.org/10.5194/acp-22-1825-2022>, 2022.

505 Chen, Y., Li, J., Lee, W., Diner, D., Garay, M., Jiang, J., Wang, Y., Yu, J., and Kalashnikova, O.:  
506 Evaluation of sea salt aerosols in climate systems: global climate modeling and observation-based  
507 analyses, *Environ. Res. Lett.*, 15, 034047, <https://doi.org/10.1088/1748-9326/ab751c>, 2020.

508 Chen, Z., Liu, J. F., Tao, W., and Tao, S.: Spatiotemporal distribution and source attribution of SOA in  
509 China, *Huan Jing Ke Xue*, 37, 2815-2822, <https://doi.org/10.13227/j.hjlx.2016.08.001>, 2016.

510 Cherian, R. and Quaas, J.: Trends in AOD, Clouds, and Cloud Radiative Effects in Satellite Data and

511 CMIP5 and CMIP6 Model Simulations Over Aerosol Source Regions, *Geophys. Res. Lett.*, 47,  
512 e2020GL087132, <https://doi.org/10.1029/2020GL087132>, 2020.

513 de Leeuw, G., Fan, C., Li, Z., Dong, J., Li, Y., Ou, Y., and Zhu, S.: Spatiotemporal variation and provincial  
514 scale differences of the AOD across China during 2000–2021, *Atmos. Pollut. Res.*, 13, 101359,  
515 <https://doi.org/10.1016/j.apr.2022.101359>, 2022.

516 Digby, R., Gillett, N., Monahan, A., von Salzen, K., Gkikas, A., Song, Q., and Zhang, Z.: How well do  
517 Earth system models reproduce the observed aerosol response to rapid emission reductions? A COVID-  
518 19 case study, *Atmos. Chem. Phys.*, 24, 2077-2097, <https://doi.org/10.5194/acp-24-2077-2024>, 2024.

519 Dunne, J. P., Horowitz, L. W., Adcroft, A. J., Ginoux, P., Held, I. M., John, J. G., Krasting, J. P., Malyshev,  
520 S., Naik, V., Paulot, F., Shevliakova, E., Stock, C. A., Zadeh, N., Balaji, V., Blanton, C., Dunne, K. A.,  
521 Dupuis, C., Durachta, J., Dussin, R., Gauthier, P. P. G., Griffies, S. M., Guo, H., Hallberg, R. W., Harrison,  
522 M., He, J., Hurlin, W., McHugh, C., Menzel, R., Milly, P. C. D., Nikonov, S., Paynter, D. J., Ploshay, J.,  
523 Radhakrishnan, A., Rand, K., Reichl, B. G., Robinson, T., Schwarzkopf, D. M., Sentman, L. T.,  
524 Underwood, S., Vahlenkamp, H., Winton, M., Wittenberg, A. T., Wyman, B., Zeng, Y., and Zhao, M.:  
525 The GFDL Earth System Model Version 4.1 (GFDL-ESM 4.1): Overall Coupled Model Description and  
526 Simulation Characteristics, *J. Adv. Model. Earth Syst.*, 12, e2019MS002015,  
527 <https://doi.org/10.1029/2019MS002015>, 2020.

528 Evan, A. T., Flamant, C., Gaetani, M., and Guichard, F.: The past, present and future of African dust,  
529 *Nature*, 531, 493-495, <https://doi.org/10.1038/nature17149> 2016.

530 Eyring, V., Bony, S., Meehl, G. A., Senior, C. A., Stevens, B., Stouffer, R. J., and Taylor, K. E.: Overview  
531 of the Coupled Model Intercomparison Project Phase 6 (CMIP6) experimental design and organization,  
532 *Geosci. Model Dev.*, 9, 1937-1958, <https://doi.org/10.5194/gmd-9-1937-2016>, 2016.

533 Fan, T., Liu, X., Wu, C., Zhang, Q., Zhao, C., Yang, X., and Li, Y.: Comparison of the Anthropogenic  
534 Emission Inventory for CMIP6 Models with a Country-Level Inventory over China and the Simulations  
535 of the Aerosol Properties, *Adv. Atmos. Sci.*, 39, 80-96, <https://doi.org/10.1007/s00376-021-1119-6>, 2022.

536 Fan, T., Zhao, C., Dong, X., Liu, X., Yang, X., Zhang, F., Shi, C., Wang, Y., and Wu, F.: Quantify  
537 contribution of aerosol errors to cloud fraction biases in CMIP5 Atmospheric Model Intercomparison  
538 Project simulations, *Int. J. Climatol.*, 38, 3140-3156, <https://doi.org/10.1002/joc.5490>, 2018a.

539 Fan, T., Liu, X., Ma, P., Zhang, Q., Li, Z., Jiang, Y., Zhang, F., Zhao, C., Yang, X., Wu, F., and Wang, Y.:  
540 Emission or atmospheric processes? An attempt to attribute the source of large bias of aerosols in eastern  
541 China simulated by global climate models, *Atmos. Chem. Phys.*, 18, 1395-1417,  
542 <https://doi.org/10.5194/acp-18-1395-2018>, 2018b.

543 Feng, L., Smith, S. J., Braun, C., Crippa, M., Gidden, M. J., Hoesly, R., Klimont, Z., van Marle, M., van  
544 den Berg, M., and van der Werf, G. R.: The generation of gridded emissions data for CMIP6, *Geosci.*  
545 *Model Dev.*, 13, 461-482, <https://doi.org/10.5194/gmd-13-461-2020>, 2020.

546 Fountoukis, C. and Nenes, A.: ISORROPIA II: a computationally efficient thermodynamic equilibrium  
547 model for K<sup>+</sup>-Ca<sup>2+</sup>-Mg<sup>2+</sup>-NH<sub>4</sub><sup>+</sup>-Na<sup>+</sup>-SO<sub>4</sub><sup>2-</sup>-NO<sub>3</sub><sup>-</sup>-Cl<sup>-</sup>-H<sub>2</sub>O aerosols, *Atmos. Chem. Phys.*, 7, 4639-

548 4659, <https://doi.org/10.5194/acp-7-4639-2007>, 2007.

549 Geng, G., Xiao, Q., Liu, S., Liu, X., Cheng, J., Zheng, Y., Xue, T., Tong, D., Zheng, B., Peng, Y., Huang,  
550 X., He, K., and Zhang, Q.: Tracking Air Pollution in China: Near Real-Time PM<sub>2.5</sub> Retrievals from  
551 Multisource Data Fusion, *Environ. Sci. Technol.*, 55, 12106-12115,  
552 <https://doi.org/10.1021/acs.est.1c01863>, 2021.

553 Hammer, M. S., van Donkelaar, A., Li, C., Lyapustin, A., Sayer, A. M., Hsu, N. C., Levy, R. C., Garay,  
554 M. J., Kalashnikova, O. V., Kahn, R. A., Brauer, M., Apte, J. S., Henze, D. K., Zhang, L., Zhang, Q.,  
555 Ford, B., Pierce, J. R., and Martin, R. V.: Global Estimates and Long-Term Trends of Fine Particulate  
556 Matter Concentrations (1998–2018), *Environ. Sci. Technol.*, 54, 7879-7890,  
557 <https://doi.org/10.1021/acs.est.0c01764>, 2020.

558 Hoesly, R. M., Smith, S. J., Feng, L., Klimont, Z., Janssens-Maenhout, G., Pitkanen, T., Seibert, J. J., Vu,  
559 L., Andres, R. J., Bolt, R. M., Bond, T. C., Dawidowski, L., Kholod, N., Kurokawa, J. I., Li, M., Liu, L.,  
560 Lu, Z., Moura, M. C. P., O'Rourke, P. R., and Zhang, Q.: Historical (1750–2014) anthropogenic emissions  
561 of reactive gases and aerosols from the Community Emissions Data System (CEDS), *Geosci. Model Dev.*,  
562 11, 369-408, <https://doi.org/10.5194/gmd-11-369-2018>, 2018.

563 Huang, Y., Shen, H., Chen, Y., Zhong, Q., Chen, H., Wang, R., Shen, G., Liu, J., Li, B., and Tao, S.:  
564 Global organic carbon emissions from primary sources from 1960 to 2009, *Atmos. Environ.*, 122, 505-  
565 512, <https://doi.org/10.1016/j.atmosenv.2015.10.017>, 2015.

566 Jacob, D. J.: Heterogeneous chemistry and tropospheric ozone, *Atmos. Environ.*, 34, 2131-2159,  
567 [https://doi.org/10.1016/S1352-2310\(99\)00462-8](https://doi.org/10.1016/S1352-2310(99)00462-8), 2000.

568 Li, K., Jacob, D. J., Liao, H., Zhu, J., Shah, V., Shen, L., Bates, K. H., Zhang, Q., and Zhai, S.: A two-  
569 pollutant strategy for improving ozone and particulate air quality in China, *Nat. Geosci.*, 12, 906-910,  
570 <https://doi.org/10.1038/s41561-019-0464-x>, 2019.

571 Li, R., Ma, X., Xiong, F., Jia, H., Sha, T., and Tian, R.: Comparisons and evaluation of aerosol burden  
572 and optical depth in CMIP5 simulations over East Asia, *J. Atmos. Solar-Terr. Phys.*, 206, 105315,  
573 <https://doi.org/10.1016/j.jastp.2020.105315>, 2020.

574 Li, X., Liu, Y., Wang, M., Jiang, Y., and Dong, X.: Assessment of the Coupled Model Intercomparison  
575 Project phase 6 (CMIP6) Model performance in simulating the spatial-temporal variation of aerosol  
576 optical depth over Eastern Central China, *Atmos. Res.*, 261, 105747,  
577 <https://doi.org/10.1016/j.atmosres.2021.105747>, 2021.

578 Lin, J., Liu, Z., Zhang, Q., Liu, H., Mao, J., and Zhuang, G.: Modeling uncertainties for tropospheric  
579 nitrogen dioxide columns affecting satellite-based inverse modeling of nitrogen oxides emissions, *Atmos.*  
580 *Chem. Phys.*, 12, 12255-12275, <https://doi.org/10.5194/acp-12-12255-2012>, 2012.

581 Lin, J., Tong, D., Davis, S., Ni, R., Tan, X., Pan, D., Zhao, H., Lu, Z., Streets, D., Feng, T., Zhang, Q.,  
582 Yan, Y., Hu, Y., Li, J., Liu, Z., Jiang, X., Geng, G., He, K., Huang, Y., and Guan, D.: Global climate  
583 forcing of aerosols embodied in international trade, *Nat. Geosci.*, 9, 790-794,  
584 <https://doi.org/10.1038/ngeo2798>, 2016.

585 Liu, R. and Liao, H.: Assessment of aerosol effective radiative forcing and surface air temperature  
586 response over eastern China in CMIP5 models, *Atmos. Oceanic Sci. Lett.*, 10, 228-234,  
587 <https://doi.org/10.1080/16742834.2017.1301188>, 2017.

588 Ma, X., Yan, P., Zhao, T., Jia, X., Jiao, J., Ma, Q., Wu, D., Shu, Z., Sun, X., and Habtemicheal, B. A.:  
589 Evaluations of Surface PM10 Concentration and Chemical Compositions in MERRA-2 Aerosol  
590 Reanalysis over Central and Eastern China, *Remote Sens.*, 13, 1317, <https://doi.org/10.3390/rs13071317>,  
591 2021.

592 Mahesh, B., Rama, B. V., Spandana, B., Sarma, M. S. S. R. K. N., Niranjana, K., and Sreekanth, V.:  
593 Evaluation of MERRAero PM<sub>2.5</sub> over Indian cities, *Adv. Space Res.*, 64, 328-334,  
594 <https://doi.org/10.1016/j.asr.2019.04.026>, 2019.

595 McDuffie, E. E., Smith, S. J., O'Rourke, P., Tibrewal, K., Venkataraman, C., Marais, E. A., Zheng, B.,  
596 Crippa, M., Brauer, M., and Martin, R. V.: A global anthropogenic emission inventory of atmospheric  
597 pollutants from sector- and fuel-specific sources (1970–2017): an application of the Community  
598 Emissions Data System (CEDS), *Earth Syst. Sci. Data*, 12, 3413-3442, [https://doi.org/10.5194/essd-12-](https://doi.org/10.5194/essd-12-3413-2020)  
599 [3413-2020](https://doi.org/10.5194/essd-12-3413-2020), 2020.

600 Metzger, S., Dentener, F., Pandis, S., and Lelieveld, J.: Gas/aerosol partitioning: 1. A computationally  
601 efficient model, *J. Geophys. Res. Atmos.*, 107, ACH 16-11-ACH 16-24,  
602 <https://doi.org/10.1029/2001JD001102>, 2002.

603 Michou, M., Nabat, P., Saint-Martin, D., Bock, J., Decharme, B., Mallet, M., Roehrig, R., Séférian, R.,  
604 Sénési, S., and Voltaire, A.: Present-Day and Historical Aerosol and Ozone Characteristics in CNRM  
605 CMIP6 Simulations, *J. Adv. Model. Earth Syst.*, 12, e2019MS001816,  
606 <https://doi.org/10.1029/2019MS001816>, 2020.

607 Mortier, A., Gliß, J., Schulz, M., Aas, W., Andrews, E., Bian, H., Chin, M., Ginoux, P., Hand, J., Holben,  
608 B., Zhang, H., Kipling, Z., Kirkevåg, A., Laj, P., Lurton, T., Myhre, G., Neubauer, D., Olivie, D., von  
609 Salzen, K., Skeie, R. B., Takemura, T., and Tilmes, S.: Evaluation of climate model aerosol trends with  
610 ground-based observations over the last 2 decades – an AeroCom and CMIP6 analysis, *Atmos. Chem.*  
611 *Phys.*, 20, 13355-13378, <https://doi.org/10.5194/acp-20-13355-2020>, 2020.

612 Mulcahy, J. P., Johnson, C., Jones, C. G., Povey, A. C., Scott, C. E., Sellar, A., Turnock, S. T., Woodhouse,  
613 M. T., Abraham, N. L., Andrews, M. B., Bellouin, N., Browse, J., Carslaw, K. S., Dalvi, M., Folberth, G.  
614 A., Glover, M., Grosvenor, D. P., Hardacre, C., Hill, R., Johnson, B., Jones, A., Kipling, Z., Mann, G.,  
615 Mollard, J., O'Connor, F. M., Palmieri, J., Reddington, C., Rumbold, S. T., Richardson, M., Schutgens,  
616 N. A. J., Stier, P., Stringer, M., Tang, Y., Walton, J., Woodward, S., and Yool, A.: Description and  
617 evaluation of aerosol in UKESM1 and HadGEM3-GC3.1 CMIP6 historical simulations, *Geosci. Model*  
618 *Dev.*, 13, 6383-6423, <https://doi.org/10.5194/gmd-13-6383-2020>, 2020.

619 Park, H., Chung, C. E., Ekman, A. M. L., and Choi, J.-O.: Evaluation of ACCMIP simulated fine-mode  
620 AOD and its implication for aerosol direct forcing, *Asia Pac. J. Atmos. Sci.*, 50, 377-390,  
621 <https://doi.org/10.1007/s13143-014-0025-6>, 2014.

622 Paulot, F., Paynter, D., Ginoux, P., Naik, V., and Horowitz, L. W.: Changes in the aerosol direct radiative  
623 forcing from 2001 to 2015: observational constraints and regional mechanisms, *Atmos. Chem. Phys.*, 18,  
624 13265-13281, <https://doi.org/10.5194/acp-18-13265-2018>, 2018.

625 Paulot, F., Ginoux, P., Cooke, W. F., Donner, L. J., Fan, S., Lin, M. Y., Mao, J., Naik, V., and Horowitz,  
626 L. W.: Sensitivity of nitrate aerosols to ammonia emissions and to nitrate chemistry: implications for  
627 present and future nitrate optical depth, *Atmos. Chem. Phys.*, 16, 1459-1477, [https://doi.org/10.5194/acp-](https://doi.org/10.5194/acp-16-1459-2016)  
628 [16-1459-2016](https://doi.org/10.5194/acp-16-1459-2016), 2016.

629 Pu, B. and Ginoux, P.: How reliable are CMIP5 models in simulating dust optical depth?, *Atmos. Chem.*  
630 *Phys.*, 18, 12491-12510, <https://doi.org/10.5194/acp-18-12491-2018>, 2018.

631 Seinfeld, J. H., Bretherton, C., Carslaw, K. S., Coe, H., DeMott, P. J., Dunlea, E. J., Feingold, G., Ghan,  
632 S., Guenther, A. B., Kahn, R., Kraucunas, I., Kreidenweis, S. M., Molina, M. J., Nenes, A., Penner, J. E.,  
633 Prather, K. A., Ramanathan, V., Ramaswamy, V., Rasch, P. J., Ravishankara, A. R., Rosenfeld, D.,  
634 Stephens, G., and Wood, R.: Improving our fundamental understanding of the role of aerosol–cloud  
635 interactions in the climate system, *P. Natl. Acad. Sci. USA*, 113, 5781-5790,  
636 <https://doi.org/10.1073/pnas.1514043113>, 2016.

637 Shim, S., Sung, H., Kwon, S., Kim, J., Lee, J., Sun, M., Song, J., Ha, J., Byun, Y., Kim, Y., Turnock, S.  
638 T., Stevenson, D. S., Allen, R. J., O'Connor, F. M., Teixeira, J. C., Williams, J., Johnson, B., Keeble, J.,  
639 Mulcahy, J., and Zeng, G.: Regional Features of Long-Term Exposure to PM<sub>2.5</sub> Air Quality over Asia  
640 under SSP Scenarios Based on CMIP6 Models, *Int. J. Environ. Res. Public Health*, 18, 6817,  
641 <https://doi.org/10.3390/ijerph18136817>, 2021.

642 Sockol, A. and Small Griswold, J. D.: Intercomparison between CMIP5 model and MODIS satellite-  
643 retrieved data of aerosol optical depth, cloud fraction, and cloud-aerosol interactions, *Earth Space Sci.*,  
644 4, 485-505, <https://doi.org/10.1002/2017EA000288>, 2017.

645 Song, H., Zhang, K., Piao, S., and Wan, S.: Spatial and temporal variations of spring dust emissions in  
646 northern China over the last 30 years, *Atmos. Environ.*, 126, 117-127,  
647 <https://doi.org/10.1016/j.atmosenv.2015.11.052>, 2016.

648 Su, X., Wu, T., Zhang, J., Zhang, Y., Jin, J., Zhou, Q., Zhang, F., Liu, Y., Zhou, Y., Zhang, L., Turnock,  
649 S. T., and Furtado, K.: Present-Day PM<sub>2.5</sub> over Asia: Simulation and Uncertainty in CMIP6 ESMs, *J.*  
650 *Meteorol. Res.*, 36, 429-449, <https://doi.org/10.1007/s13351-022-1202-7>, 2022.

651 Tang, Z., Tian, J., Zhang, Y., Zhang, X., Zhang, J., Ma, N., Li, X., and Song, P.: Anthropogenic aerosols  
652 dominated the decreased solar radiation in eastern China over the last five decades, *J. Clean. Prod.*, 380,  
653 135150, <https://doi.org/10.1016/j.jclepro.2022.135150>, 2022.

654 Tao, S., Ru, M. Y., Du, W., Zhu, X., Zhong, Q. R., Li, B. G., Shen, G. F., Pan, X. L., Meng, W. J., Chen,  
655 Y. L., Shen, H. Z., Lin, N., Su, S., Zhuo, S. J., Huang, T. B., Xu, Y., Yun, X., Liu, J. F., Wang, X. L., Liu,  
656 W. X., Cheng, H. F., and Zhu, D. Q.: Quantifying the rural residential energy transition in China from  
657 1992 to 2012 through a representative national survey, *Nat. Energy*, 3, 567-573,  
658 <https://doi.org/10.1038/s41560-018-0158-4>, 2018.

659 Tegen, I., Neubauer, D., Ferrachat, S., Siegenthaler-Le Drian, C., Bey, I., Schutgens, N., Stier, P., Watson-  
660 Parris, D., Stanelle, T., Schmidt, H., Rast, S., Kokkola, H., Schultz, M., Schroeder, S., Daskalakis, N.,  
661 Barthel, S., Heinold, B., and Lohmann, U.: The global aerosol–climate model ECHAM6.3–HAM2.3 –  
662 Part 1: Aerosol evaluation, *Geosci. Model Dev.*, 12, 1643-1677, [https://doi.org/10.5194/gmd-12-1643-](https://doi.org/10.5194/gmd-12-1643-2019)  
663 [2019](https://doi.org/10.5194/gmd-12-1643-2019), 2019.

664 Turnock, S. T., Allen, R. J., Andrews, M., Bauer, S. E., Deushi, M., Emmons, L., Good, P., Horowitz, L.,  
665 John, J. G., Michou, M., Nabat, P., Naik, V., Neubauer, D., O'Connor, F. M., Olivie, D., Oshima, N.,  
666 Schulz, M., Sellar, A., Shim, S., Takemura, T., Tilmes, S., Tsigaridis, K., Wu, T., and Zhang, J.: Historical  
667 and future changes in air pollutants from CMIP6 models, *Atmos. Chem. Phys.*, 20, 14547-14579,  
668 <https://doi.org/10.5194/acp-20-14547-2020>, 2020.

669 van Donkelaar, A., Martin, R. V., Li, C., and Burnett, R. T.: Regional Estimates of Chemical Composition  
670 of Fine Particulate Matter Using a Combined Geoscience-Statistical Method with Information from  
671 Satellites, Models, and Monitors, *Environ. Sci. Technol.*, 53, 2595-2611,  
672 <https://doi.org/10.1021/acs.est.8b06392>, 2019.

673 van Donkelaar, A., Martin, R. V., Brauer, M., Hsu, N. C., Kahn, R. A., Levy, R. C., Lyapustin, A., Sayer,  
674 A. M., and Winker, D. M.: Global Estimates of Fine Particulate Matter using a Combined Geophysical-  
675 Statistical Method with Information from Satellites, Models, and Monitors, *Environ. Sci. Technol.*, 50,  
676 3762-3772, <https://doi.org/10.1021/acs.est.5b05833>, 2016.

677 van Donkelaar, A., Hammer, M. S., Bindle, L., Brauer, M., Brook, J. R., Garay, M. J., Hsu, N. C.,  
678 Kalashnikova, O. V., Kahn, R. A., Lee, C., Levy, R. C., Lyapustin, A., Sayer, A. M., and Martin, R. V.:  
679 Monthly Global Estimates of Fine Particulate Matter and Their Uncertainty, *Environ. Sci. Technol.*, 55,  
680 15287-15300, <https://doi.org/10.1021/acs.est.1c05309>, 2021.

681 van Noije, T., Bergman, T., Le Sager, P., O'Donnell, D., Makkonen, R., Gonçalves-Ageitos, M., Döschner,  
682 R., Fladrich, U., von Hardenberg, J., Keskinen, J. P., Korhonen, H., Laakso, A., Myriokefalitakis, S.,  
683 Ollinaho, P., Pérez García-Pando, C., Reerink, T., Schrödner, R., Wyser, K., and Yang, S.: EC-Earth3-  
684 AerChem: a global climate model with interactive aerosols and atmospheric chemistry participating in  
685 CMIP6, *Geosci. Model Dev.*, 14, 5637-5668, <https://doi.org/10.5194/gmd-14-5637-2021>, 2021.

686 Wang, C., Wang, Z., Lei, Y., Zhang, H., Che, H., and Zhang, X.: Differences in East Asian summer  
687 monsoon responses to Asian aerosol forcing under different emission inventories, *Adv. Clim. Change*  
688 *Res.*, 13, 309-322, <https://doi.org/10.1016/j.accre.2022.02.008>, 2022.

689 Wang, R., Tao, S., Shen, H., Huang, Y., Chen, H., Balkanski, Y., Boucher, O., Ciais, P., Shen, G., Li, W.,  
690 Zhang, Y., Chen, Y., Lin, N., Su, S., Li, B., Liu, J., and Liu, W.: Trend in Global Black Carbon Emissions  
691 from 1960 to 2007, *Environ. Sci. Technol.*, 48, 6780-6787, <https://doi.org/10.1021/es5021422>, 2014.

692 Wang, S., Yu, Y., Zhang, X., Lu, H., Zhang, X., and Xu, Z.: Weakened dust activity over China and  
693 Mongolia from 2001 to 2020 associated with climate change and land-use management, *Environ. Res.*  
694 *Let.*, 16, <https://doi.org/10.1088/1748-9326/ac3b79>, 2021a.

695 Wang, Z., Lin, L., Xu, Y., Che, H., Zhang, X., Zhang, H., Dong, W., Wang, C., Gui, K., and Xie, B.:



696 Incorrect Asian aerosols affecting the attribution and projection of regional climate change in CMIP6  
697 models, *NPJ Clim. Atmos. Sci.*, 4, 2, <https://doi.org/10.1038/s41612-020-00159-2>, 2021b.

698 Wilcox, L. J., Allen, R. J., Samset, B. H., Bollasina, M. A., Griffiths, P. T., Keeble, J. M., Lund, M. T.,  
699 Makkonen, R., Merikanto, J., O'Donnell, D., Paynter, D. J., Persad, G. G., Rumbold, S. T., Takemura, T.,  
700 Tsigaridis, K., Undorf, S., and Westervelt, D. M.: The Regional Aerosol Model Intercomparison Project  
701 (RAMIP), *Geosci. Model Dev. Discuss.*, 2022, 1-40, <https://doi.org/10.5194/gmd-2022-249>, 2022.

702 World Health Organization: WHO global air quality guidelines: particulate matter (PM<sub>2.5</sub> and PM<sub>10</sub>),  
703 ozone, nitrogen dioxide, sulfur dioxide and carbon monoxide, World Health Organization,  
704 <https://apps.who.int/iris/handle/10665/345329>, 2021.

705 Wu, J., Shi, Y., and Xu, Y.: Evaluation and Projection of Surface Wind Speed Over China Based on  
706 CMIP6 GCMs, *J. Geophys. Res. Atmos.*, 125, e2020JD033611, <https://doi.org/10.1029/2020JD033611>,  
707 2020a.

708 Wu, T., Zhang, F., Zhang, J., Jie, W., Zhang, Y., Wu, F., Li, L., Yan, J., Liu, X., Lu, X., Tan, H., Zhang,  
709 L., Wang, J., and Hu, A.: Beijing Climate Center Earth System Model version 1 (BCC-ESM1): model  
710 description and evaluation of aerosol simulations, *Geosci. Model Dev.*, 13, 977-1005,  
711 <https://doi.org/10.5194/gmd-13-977-2020>, 2020b.

712 Wu, T., Lu, Y., Fang, Y., Xin, X., Li, L., Li, W., Jie, W., Zhang, J., Liu, Y., Zhang, L., Zhang, F., Zhang,  
713 Y., Wu, F., Li, J., Chu, M., Wang, Z., Shi, X., Liu, X., Wei, M., Huang, A., Zhang, Y., and Liu, X.: The  
714 Beijing Climate Center Climate System Model (BCC-CSM): the main progress from CMIP5 to CMIP6,  
715 *Geosci. Model Dev.*, 12, 1573-1600, <https://doi.org/10.5194/gmd-12-1573-2019>, 2019.

716 Xu, Y., Wu, J., and Han, Z.: Evaluation and Projection of Surface PM<sub>2.5</sub> and Its Exposure on Population  
717 in Asia Based on the CMIP6 GCMs, *Int. J. Environ. Res. Public Health*, 19, 12092,  
718 <https://doi.org/10.3390/ijerph191912092>, 2022.

719 Yang, X., Zhou, B., Xu, Y., and Han, Z.: CMIP6 Evaluation and Projection of Temperature and  
720 Precipitation over China, *Adv. Atmos. Sci.*, 38, 817-830, <https://doi.org/10.1007/s00376-021-0351-4>,  
721 2021.

722 Yue, M., Wang, M., Guo, J., Zhang, H., Dong, X., and Liu, Y.: Long-Term Trend Comparison of Planetary  
723 Boundary Layer Height in Observations and CMIP6 Models over China, *J. Clim.*, 34, 8237-8256,  
724 <https://doi.org/10.1175/JCLI-D-20-1000.1>, 2021.

725 Zhai, S., Jacob, D. J., Wang, X., Shen, L., Li, K., Zhang, Y., Gui, K., Zhao, T., and Liao, H.: Fine  
726 particulate matter (PM<sub>2.5</sub>) trends in China, 2013–2018: separating contributions from anthropogenic  
727 emissions and meteorology, *Atmos. Chem. Phys.*, 19, 11031-11041, <https://doi.org/10.5194/acp-19-11031-2019>,  
728 2019.

729 Zhai, S., Jacob, D. J., Wang, X., Liu, Z., Wen, T., Shah, V., Li, K., Moch, J. M., Bates, K. H., Song, S.,  
730 Shen, L., Zhang, Y., Luo, G., Yu, F., Sun, Y., Wang, L., Qi, M., Tao, J., Gui, K., Xu, H., Zhang, Q., Zhao,  
731 T., Wang, Y., Lee, H. C., Choi, H., and Liao, H.: Control of particulate nitrate air pollution in China, *Nat.*  
732 *Geosci.*, 14, 389-395, <https://doi.org/10.1038/s41561-021-00726-z>, 2021.



733 Zhang, L., Li, J., Jiang, Z., Dong, Y., Ying, T., and Zhang, Z.: Clear-Sky Direct Aerosol Radiative Forcing  
734 Uncertainty Associated with Aerosol Optical Properties Based on CMIP6 Models, *J. Climate*, 35, 3007-  
735 3019, <https://doi.org/10.1175/JCLI-D-21-0479.1>, 2022a.

736 Zhang, Q., Jiang, X., Tong, D., Davis, S. J., Zhao, H., Geng, G., Feng, T., Zheng, B., Lu, Z., Streets, D.  
737 G., Ni, R., Brauer, M., van Donkelaar, A., Martin, R. V., Huo, H., Liu, Z., Pan, D., Kan, H., Yan, Y., Lin,  
738 J., He, K., and Guan, D.: Transboundary health impacts of transported global air pollution and  
739 international trade, *Nature*, 543, 705-709, <https://doi.org/10.1038/nature21712>, 2017.

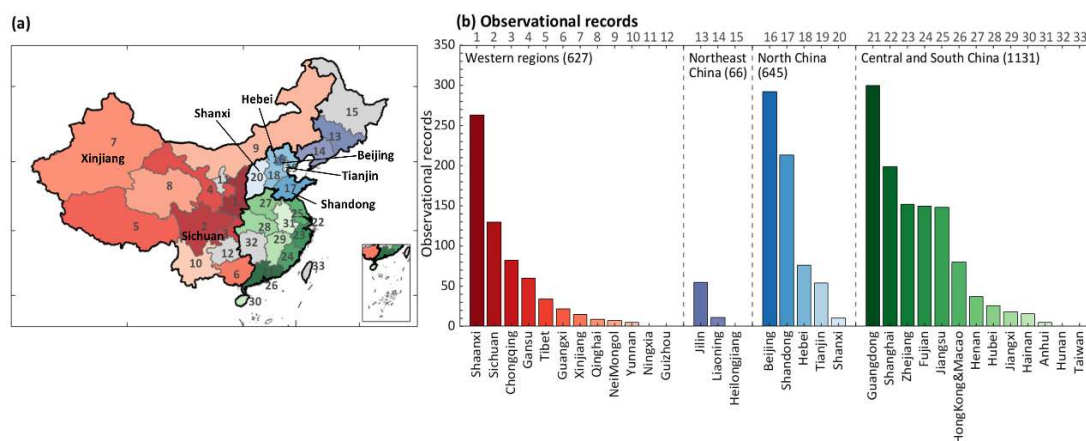
740 Zhang, X., Hua, L., and Jiang, D.: Assessment of CMIP6 model performance for temperature and  
741 precipitation in Xinjiang, China, *Atmos. Oceanic Sci. Lett.*, 15, 100128,  
742 <https://doi.org/10.1016/j.aosl.2021.100128>, 2022b.

743 Zhao, A., Ryder, C. L., and Wilcox, L. J.: How well do the CMIP6 models simulate dust aerosols?, *Atmos.*  
744 *Chem. Phys.*, 22, 2095-2119, <https://doi.org/10.5194/acp-22-2095-2022>, 2022.

745 Zheng, B., Tong, D., Li, M., Liu, F., Hong, C., Geng, G., Li, H., Li, X., Peng, L., Qi, J., Yan, L., Zhang,  
746 Y., Zhao, H., Zheng, Y., He, K., and Zhang, Q.: Trends in China's anthropogenic emissions since 2010 as  
747 the consequence of clean air actions, *Atmos. Chem. Phys.*, 18, 14095-14111, [https://doi.org/10.5194/acp-](https://doi.org/10.5194/acp-18-14095-2018)  
748 [18-14095-2018](https://doi.org/10.5194/acp-18-14095-2018), 2018.

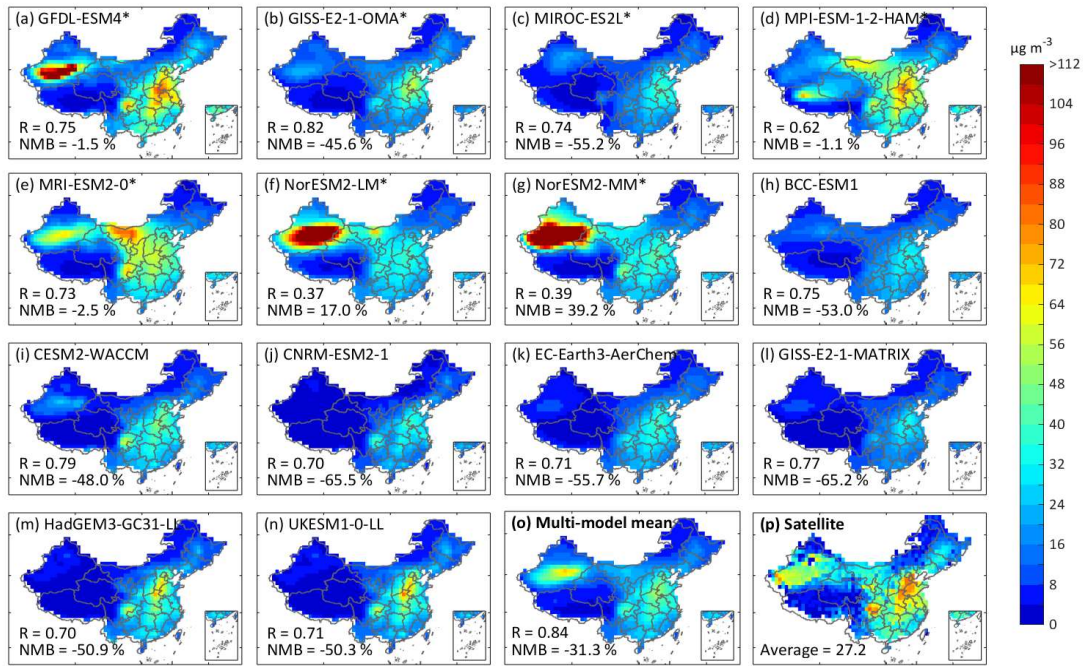
749 Zhu, H., Jiang, Z., Li, J., Li, W., Sun, C., and Li, L.: Does CMIP6 Inspire More Confidence in Simulating  
750 Climate Extremes over China?, *Adv. Atmos. Sci.*, 37, 1119-1132, [https://doi.org/10.1007/s00376-020-](https://doi.org/10.1007/s00376-020-9289-1)  
751 [9289-1](https://doi.org/10.1007/s00376-020-9289-1), 2020.

752 Zhu, Y. and Yang, S.: Evaluation of CMIP6 for historical temperature and precipitation over the Tibetan  
753 Plateau and its comparison with CMIP5, *Adv. Clim. Chang. Res.*, 11, 239-251,  
754 <https://doi.org/10.1016/j.accre.2020.08.001>, 2020.



755 **Figure 1.** Observational records of PM<sub>2.5</sub> components during 2000–2014 collected from the literature. (a) The map  
756 depicts individual provinces in four regions, including the western regions in red colors, Northeast China in purple,  
757 North China in blue, and Central and South China in green. The provinces without observational records are in gray.  
758 The number denotes each province. (b) Provincial observation records in China. The number in the upper x-axis and  
759

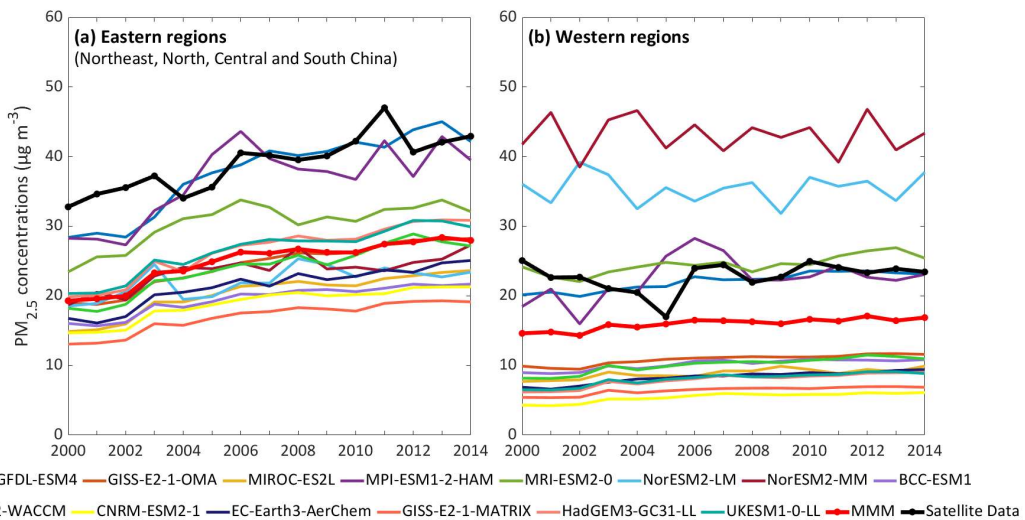
760 the color in each bar match the province in (a).



761

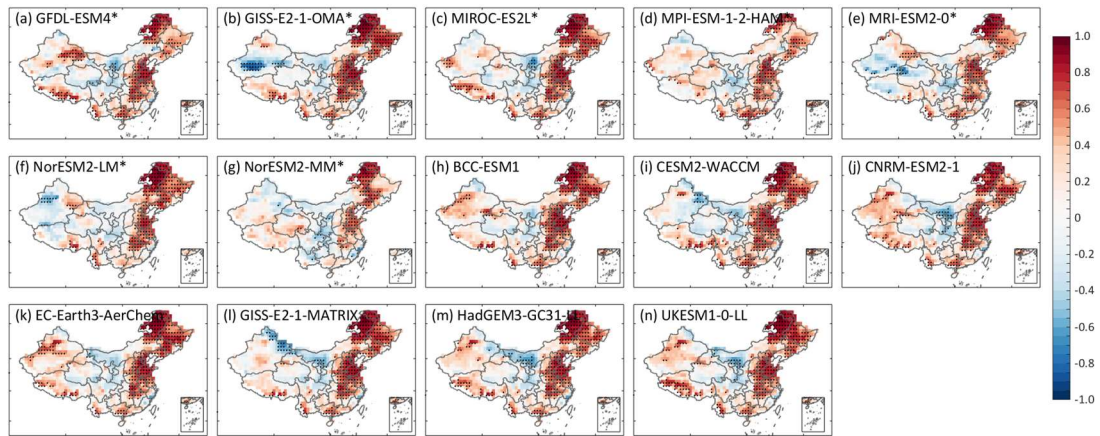
762 **Figure 2.** Multi-year mean annual average near-surface total PM<sub>2.5</sub> concentrations over China during 2000–2014.

763 (a-g) Model outputted PM<sub>2.5</sub> concentrations in seven models. (h-n) Calculated PM<sub>2.5</sub> concentrations in the other  
 764 seven models according to Eq. 1. (o) Multi-model mean. (p) Satellite-based total PM<sub>2.5</sub> dataset. R stands for spatial  
 765 correlation, and NMB stands for normalized mean bias.



766

767 **Figure 3.** Time series of annual mean regional average total PM<sub>2.5</sub> concentrations. (a) Over the eastern regions  
 768 (including Northeast China, North China, and Central and South China). (b) Over the western regions. The bold  
 769 black lines denote satellite-based PM<sub>2.5</sub> concentrations, and the bold red lines denote multi-model mean (MMM)  
 770 concentrations.



771

772

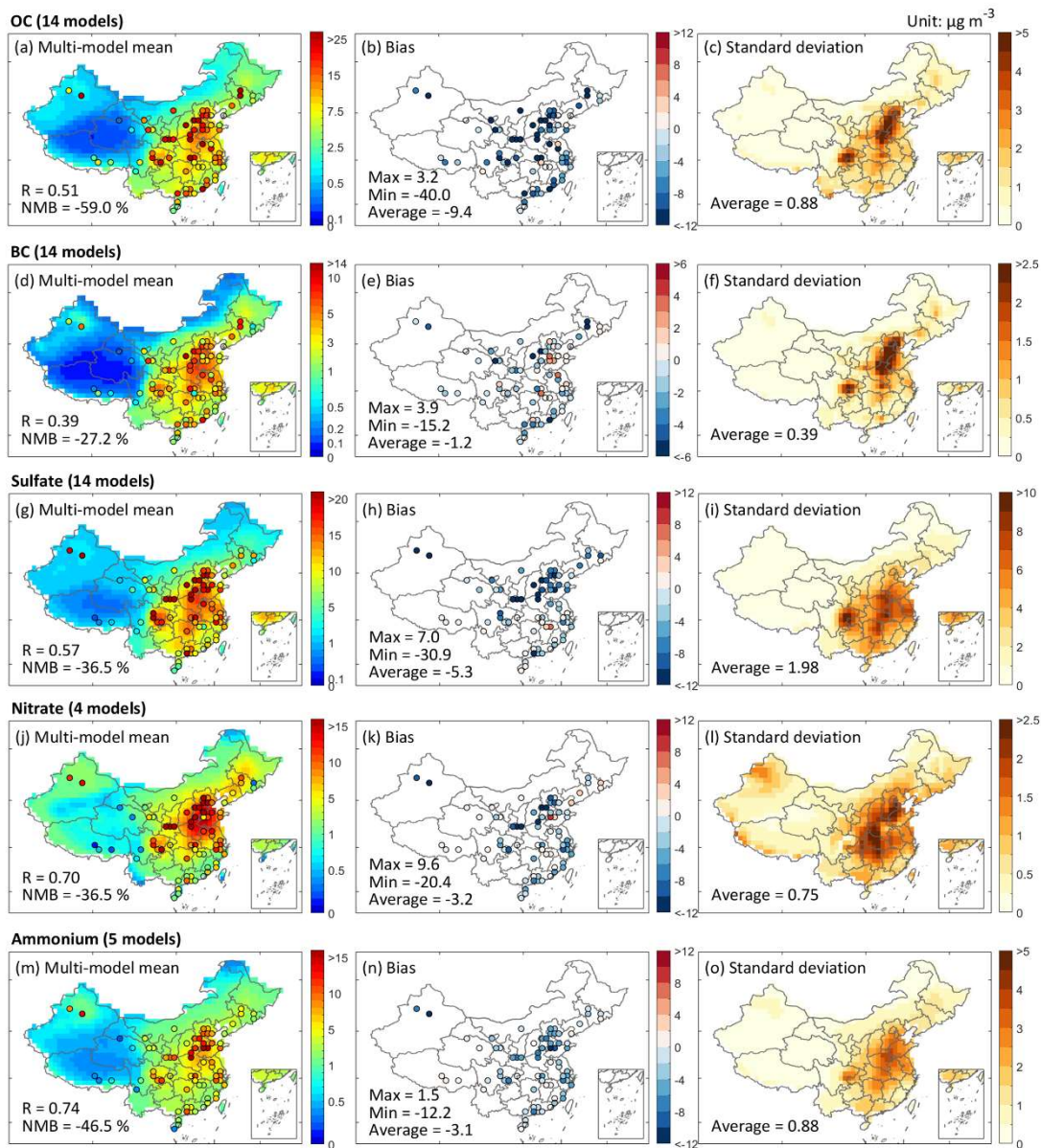
**Figure 4.** Spatial distribution of correlation coefficients between modeled and satellite-based data for interannual

773

variations of annual mean total  $PM_{2.5}$  concentrations during 2000–2014. Black dots indicate a significance level of

774

0.05.



775

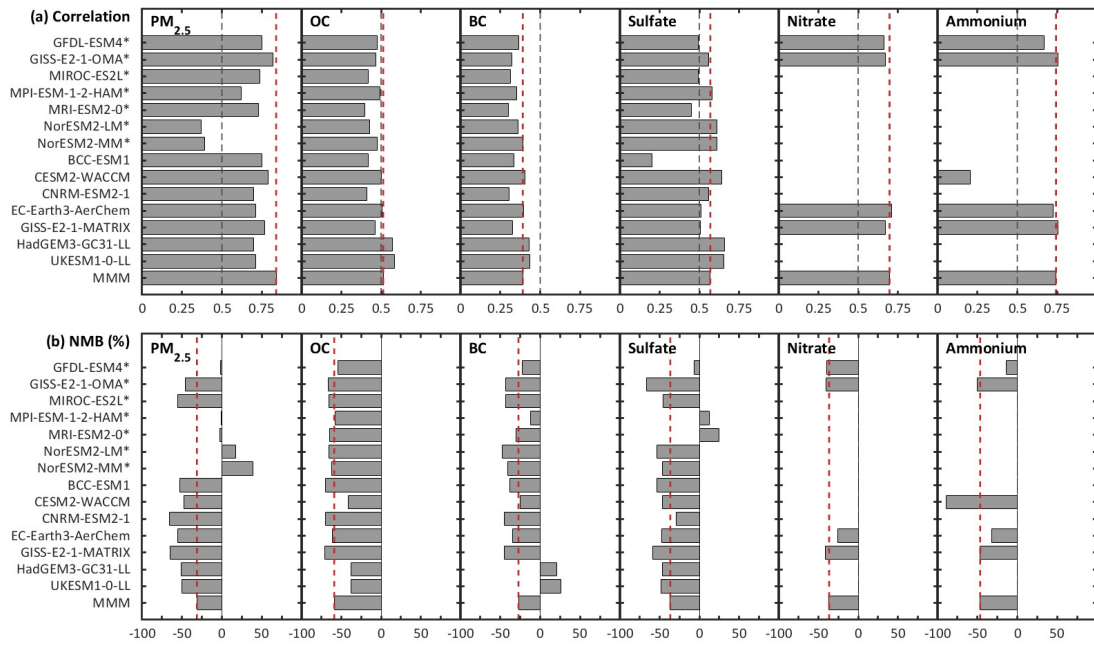
776 **Figure 5.** Spatial distribution of multi-year averages of modeled  $\text{PM}_{2.5}$  components during 2000–2014. (First column)

777 The multi-model mean  $\text{PM}_{2.5}$  component concentrations, overlaid with average ground-based observations in filled

778 circles. (Second column) The bias of multi-model mean concentrations. (Third column) The standard deviation of

779  $\text{PM}_{2.5}$  component simulations among the CMIP6 models.





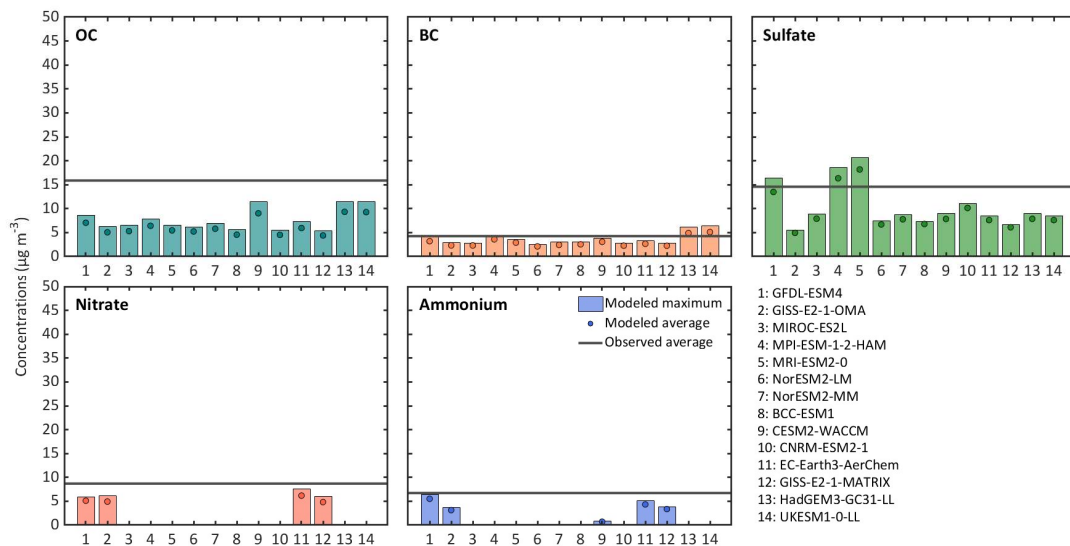
780

781 **Figure 6.** Multi-year mean spatial correlation and bias for PM<sub>2.5</sub> components over 2000–2014 for individual models.

782 Results for total PM<sub>2.5</sub> refer to the comparison against the satellite-based dataset, and those for components are

783 relative to the observations compiled from the literature. The red dotted lines denote multi-model mean (MMM).

784 The black dotted lines denote the spatial correlation coefficient value of 0.5.



785

786 **Figure 7.** Maximum and average concentrations over 2000–2014 for simulated national mean PM<sub>2.5</sub> components

787 simulated by individual models. In each year, model values are sampled from grid cells with available observations.